Dropwise Cooling: Experimental Tests by Infrared Thermography and Numerical Simulations

P. Tartarini, M.A. Corticelli, L. Tarozzi

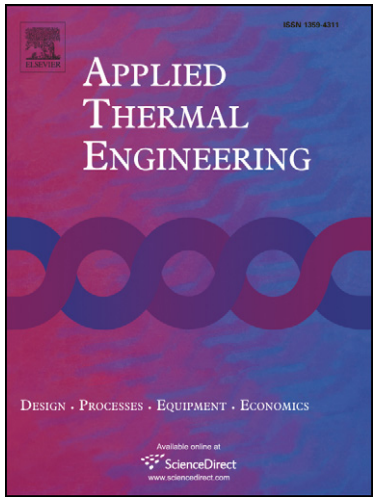

Dropwise Cooling: Experimental Tests by Infrared Thermography and Numerical Simulations

P. Tartarini, M.A. Corticelli, L. Tarozzi

PII: S1359-4311(08)00272-X
DOI: 10.1016/j.applthermaleng.2008.06.011
Reference: ATE 2542

To appear in: *Applied Thermal Engineering*

Received Date: 21 November 2007
Revised Date: 23 April 2008
Accepted Date: 10 June 2008

Please cite this article as: P. Tartarini, M.A. Corticelli, L. Tarozzi, Dropwise Cooling: Experimental Tests by Infrared Thermography and Numerical Simulations, *Applied Thermal Engineering* (2008), doi: 10.1016/j.applthermaleng.2008.06.011

DROPWISE COOLING: EXPERIMENTAL TESTS BY INFRARED THERMOGRAPHY AND NUMERICAL SIMULATIONS.

P. Tartarini*, M.A. Corticelli and L. Tarozzi

DIMeC, University of Modena and Reggio Emilia,
Via Vignolese 905, 41100 Modena, Italy,
Tel. (+39) 059-2056146; Fax (+39) 059-2056126;
*e-mail: tartarini@unimore.it

ABSTRACT

In this paper, infrared thermography is used to measure the transient contact temperature between impinging droplets and hot solid surfaces. Droplets are released onto the heated solid surface of a barium fluoride (BaF_2) disk, which has a high transmittance (about 90%) in the 8-12 μm range (typical of longwave infrared cameras). The interface temperature is measured from below, through the solid material, by infrared thermography. Since the solid is IR-transparent, a black coating layer is used to allow radiative heating of the surface and provide a method to measure the liquid-solid interface temperature. A numerical code is then presented, which simulates the evaporation of water droplets on hot solid surfaces. At the present stage of development, single-phase evaporation is addressed. The three-dimensional energy diffusion equation, discretized using the finite volume method, is employed to model the transient within both the droplets and the solid substrate. The numerical results are validated by comparison with the experimental data.

Keywords: Droplet cooling; heat transfer; infrared thermography.

INTRODUCTION

Many engineering and safety applications require that a hot surface is effectively cooled down by a spray of water droplets. Fire suppression in nuclear power plants, in process chemical storage and in fuel storage facilities is a primary application which has inspired a number of experimental and theoretical studies on the phenomena associated with spray cooling. A thorough survey of the hundreds of relevant literature works on this subject would exceed the full length of the present paper, and only some examples of important contributions will be mentioned here.

Fire protection applications are the focus of the work presented here, which has to be seen in the frame of a long-term research whose results have been published in some papers during almost two decades (di Marzo and Evans [1], di Marzo *et al.* [2,3], Tartarini and di Marzo [4], Chandra *et al.* [5], Tartarini *et al.* [6], Tarozzi *et al.* [7,8]).

The behavior of sessile droplets has been investigated extensively by several researchers. Some fundamental studies on which spray heat transfer modeling could be based are due to Gorton [9], Wachters *et al.* [10], Baumeister *et al.* [11], Bolle and Moureau [12] and Chandra and Avedisian [13]. Gorton [9] found experimentally that, in film boiling, the vapor film thickness between a sessile droplet and the surface increases and the heat transfer coefficient decreases with an increase in surface temperature. Wachters *et al.* [10] proposed a detailed discussion of the shape of a sessile drop on a horizontal, hot solid surface. Baumeister *et al.* [11] developed a dimensionless correlation for the vaporization times of discrete liquid masses in the film boiling regime. Bolle and Moureau [12] and Chandra and Avedisian [13] presented analytical methods to predict the thickness of the vapor layer separating a hemispherical liquid droplet from a hot surface during film boiling.

Also the behavior of impinging droplets has been investigated by a large number of researchers. The impact and deformation of a liquid droplet impinging upon a heated surface has been studied with heavy use of high speed photography. Among early works, Wachters and Westerling [14] observed that the impact and breakup of water droplets striking a 400°C horizontal surface (corresponding to the film boiling regime) could be grouped into three general categories depending upon the droplet Weber number, *We* (ratio of droplet inertia forces to surface tension forces). In the low Weber number regime ($We<30$), Wachters and Westerling [14] observed that the droplet was spreading out radially upon impact into a flat disk with a fairly uniform thickness, and the impact did not influence the initial shape of the droplet. During an evaporative transient in regimes of single-phase evaporation, the radius of the wetted region, R, remains constant and the solid-liquid contact angle, θ, decreases until a minimum, critical value (receding angle) is reached. Detailed information on the receding angle is available in several works (Adam and Jessop [15], Good [16], Herzberg and Marian [17], Herzberg *et al.* [18]). The evaporation process ends with the complete evaporation of the droplet, and the solid surface temperature tends to return to its initial conditions.

In the mid-Weber-number regime ($30<We\leq80$), the droplet was observed to split into a large globule and a small satellite. Finally, in the high-Weber-number regime ($We>80$), upon impact, the droplet began to spread out radially into a flat disk, the rim of which broke into several small droplets which quickly dispersed away from the rim. The flat disk itself then broke up violently into many small droplets.

While the classification by Wachters and Westerling [14] is usually accepted in the ranges of high solid surface temperatures, the droplet impact characteristics are found to be highly dependent on temperature over the ranges including single-phase evaporation

and nucleate boiling phenomena. Chandra and Avedisian [13], in their famous, comprehensive photographic study, investigated the influence of surface temperature on droplet impact dynamics. Using flash photography, they observed the liquid film spreading structure and spreading rate, vapor bubble formation, and contact angle for n-heptane droplets with *We* = 43 impinging upon a polished stainless steel surface. They showed that all these impact characteristics were highly temperature dependent over the range of 24-250°C.

The observations of Wachters and Westerling [14] in the field of high temperatures were confirmed later by Bolle and Moureau [12], who employed high-speed film-based photography (7000 frames per second) to investigate droplet impact for surface temperatures in the range of 800-1200°C (film boiling regime) and *We* of 1-1500. Extensive contributions in this field are also available in the excellent papers by Bernardin and Mudawar [19] and Bernardin *et al.* [20].

Recent improvements of photographic techniques allowed some authors to obtain excellent results in terms of droplet impact visualization. Two relevant contributions in this field are the papers by Sikalo *et al.* [21] and Cossali *et al.* [22]. Cossali *et al.* [22] used a CCD camera with a long distance microscope objective to acquire the images of droplet impacts. The CCD acquisition and illumination systems were driven by a triggering system made by an He–Ne laser imaged onto a photodiode.

In terms of solid heating modes, when the solid surface is heated by conduction from below, the solid layer under the droplet(s) acts as a heat source, while it is a heat sink when the solid surface is heated by radiation from above. Moreover, in the radiative case the droplets absorb heat directly from ambient, and their surface tension is strongly decreased. The two described scenarios are interesting and important in industrial and civil engineering applications.

The present work is aimed at analyzing the cooling of hot solid surfaces induced by liquid droplets. In particular, the study is focused on non-intrusive measurements and numerical simulations of the transient behavior of the contact temperature between impinging droplets and hot solid surfaces.

EXPERIMENTAL APPARATUS AND RESULTS

In order to overcome the measurement difficulties regarding the liquid-solid interface temperature without using direct-contact sensors, a new method was devised to measure the interface temperature without contact, releasing the droplets onto a heated solid surface of a material transparent in the infrared spectral band. Therefore, the experimental apparatus was built to measure the temperature at the solid-liquid interface during evaporation of liquid droplets on a horizontal solid surface heated by radiation from above, and the interface temperature could be measured from below, through the solid material, by infrared thermography. Since the solid was IR-transparent, a coating layer was used to allow radiative heating of the solid surface and provide a method to visualize the bottom surface temperature, which was *de facto* undistinguishable from the solid-liquid interface temperature.

The full experimental apparatus and setup is thoroughly described in published papers by Tarozzi *et al.* [7,8]. However, it is worth reminding that the IR-transparent material is a disk of barium fluoride (BaF_2, Crystran Ltd. [23]) with a diameter of 75 mm and a thickness of 3 mm, which is mounted on a horizontal slab of insulating material. A circular window is opened through the slab and is filled by the transparent disk in order to avoid radial heat losses and insure homogeneous heating of the BaF_2 disk. Droplets of bidistilled and deionized water are gently deposited (the Weber number is always less than 30 in this part of the research) by a precision syringe onto the upper surface of the heated disk.

A picture of the experimental apparatus and a sketch of the test section are reported in Figs. 1 and 2 respectively. Additionally, a sketch of the test section, including sizes and measurements, is reported in Fig. 3.

The interface temperature is measured from below, through the solid material, by an Avio TVS-500 thermographic camera, carrying a micro-bolometric FPA sensor which operates in the long-wave spectral range (8-12 μm). The camera features an IEEE-1394 interface, which allows one to export up to 60 frames per second to a personal computer. The infrared frame sequences are then processed by the Matlab® software, in order to enhance the image quality by noise filtering and emissivity maps.

An improvement with respect to previous experiments by Tarozzi *et al.* [7] was obtained by using a close-up lens. This enhancement of the setup now allows one to acquire thermographic images with a spatial resolution of 100 μm/pixel, thus obtaining several tens of pixels along the droplet diameter.

The top surfaces of both disk and slab are heated from above by four radiant panels; the heating is active during the deposition of the droplets and the entire evaporation period. The panels are fed by a three-phase power supply which is controlled on a temperature feedback by a Variac. This allows one to modulate the radiant flux and, therefore, the initial surface temperature by varying the electric tension. A homogeneous irradiation is achieved by modifying the position of each heater independently. A uniform heating was easily achieved during the tests. The temperature uniformity of the test section has been verified by means of thermographic images.

The solid disk of barium fluoride is transparent to infrared radiation. Therefore, a coating layer has to be used to get radiative heating of the solid surface. Thanks to the same coating layer the solid-liquid interface temperature can be measured. In fact, the temperature that the infrared camera measures through the transparent disk is that of the bottom surface of the coating layer, i.e. at the coating-solid interface, but this can be assumed to be equal to the solid-liquid interface temperature if the coating layer is thin

and conductive enough.

The main component of the apparatus is the BaF_2 disk, transparent in the infrared spectral band, on which the droplets are deposited. The optical properties of the disk were not released by the producer. Thus, its transmittance had to be measured over the whole range of the spectrum relevant to thermal radiation, in order to verify the compatibility with the employed infrared camera. A Bruker Vertex 70 FTIR spectrophotometer was used, which provided the Fourier Transform Infrared Spectrophotometry (FTIR) to determine the spectral transmittance of materials. The measurement results are reported in Fig. 4, which shows an average transmittance of about 0.90% in the spectral range of interest (8-12 μm), as confirmed by thermographic analyses of objects with known temperature.

No significant effects of the disk temperature on its radiative properties were observed in the temperature range of interest.

The IR camera measures the thermal radiation which leaves the uncoated bottom surface of the disk. More precisely, the camera measures the fraction of the thermal radiation comprised in the spectral range $\Delta\lambda$=8-12 μm. This includes the thermal radiation emitted by the top coating layer and transmitted through the disk, and the thermal radiation emitted by the bottom surface of the disk.

With a temperature of the coating layer equal to that of the disk bottom, the camera measures a blackbody radiation, i.e., the apparent emissivity of the coating layer is 1. This was verified by comparing the coating temperature measured thermographically from below with the temperature measured by a direct-contact thermocouple probe applied to the upper coated surface.

Water droplets were gently deposited (the Weber number was always less than 30)

on the coated surface of the disk, which was heated up to prescribed values of temperature. This solid surface temperature T_s was chosen according to the theoretical contact temperature proposed by Seki *et al.* [24] on the basis of the classical work by Carslaw and Jaeger [25], who developed it as the weighted average of liquid and solid effusivities by similarity with two semi-infinite solids in contact:

$$T_{contact} = \frac{T_s\sqrt{\rho_s c_s k_s} + T_l\sqrt{\rho_l c_l k_l}}{\sqrt{\rho_s c_s k_s} + \sqrt{\rho_l c_l k_l}} \quad (1)$$

where ρ, c and k are the mass density, the specific heat and the thermal conductivity, respectively, the subscripts s and l denote the solid surface and the liquid, and T_s and T_l are the temperatures of solid and liquid.

Since the droplets were always released at ambient temperature (i.e., $T_l = 20°C$ at t = 0), the initial solid surface temperature could also be used as the forcing parameter to get $T_{contact}$ close to the saturation temperature of the liquid and check the transient cooling behavior before and after the onset of nucleate boiling within a droplet.

Figure 5 reports two frames of a sequence of the evaporation of four distinct droplets (45 µl each) on the BaF_2 disk at $T_0 = 97°C$. Figure 6 reports two frames of a sequence of the evaporation of a multi-droplet spray (180 µl, with an experimental uncertainty of 20 µl) at $T_0 = 97°C$. Figure 7 shows the comparison between experimental and predicted values of temperature vs. time on the wetted area only, using the old assumption of constant and uniform $T_{contact}$ in Eq. (1). The comparison suggests that $T_{contact}$ could be used as an integral-averaged value of the interface temperature, but the experiments clearly confirm (Abu-Zaid and Atreya [26], di Marzo *et al.* [3] Tartarini and di Marzo [4]) that the theoretical contact temperature is not constant nor uniform during an evaporative transient on low- and mid-conductivity solid surfaces.

NUMERICAL APPROACH AND PRELIMINARY RESULTS

In previous attempts of modeling single-phase droplet cooling after the work by Rizza [27], di Marzo *et al.* [3] and Tartarini and di Marzo [4] demonstrated that conduction is the dominant heat transfer mode inside the droplets in the low superheat regime. After carrying out extensive experimental research, they formulated a numerical code for the prediction of evaporative cooling of solid surfaces induced by a gently deposited water droplet. The code was based upon a solid-liquid coupled model which predicted the droplet evaporation and the solid surface cooling for materials with thermal conductivity spanning over more than two orders of magnitude. The numerical solution of the conduction equation linked a control volume method (CVM) used for the liquid and a boundary element method (BEM, as in Wrobel and Brebbia [28]) used for the solid. The numerical predictions by that code were in very good agreement with the experimental data, in terms of both evaporation times (lifetimes) and solid surface temperatures. That code was very effective, but it could not simulate the three-dimensional behavior of evaporative cooling in higher superheat regimes. The present modeling effort tries to overcome that problem, thanks to the enhanced computational capabilities of modern machines.

A new numerical code is now presented, which simulates the evaporation of water droplets on hot solid surfaces. The three-dimensional, energy diffusion equation, discretized using the finite volume method, is employed to model the transient within both the droplets and the solid substrate. In this preliminary stage of development, the new code can simulate the substrate cooling effect due to a droplet in the single-phase evaporation regime only, but its structure permits an easy extension to nucleate boiling

and film boiling regimes. The code is implemented in Matlab®, using a modular and flexible architecture.

The thermal behavior of both liquid droplets and solid substrate is described by the Fourier equation of heat diffusion:

$$\frac{\partial T_l}{\partial t} = \alpha_l \nabla^2 T_l \tag{2}$$

$$\frac{\partial T_s}{\partial t} = \alpha_s \nabla^2 T_s \tag{3}$$

The vapor mass flux m" at the liquid-air interface, due to the droplet evaporation, can be estimated by the classical correlation due to Chilton and Colburn [29]:

$$m'' = 0.624 \cdot h \cdot \left(\frac{d_{aw}}{\alpha_a} \right)^{\frac{2}{3}} \frac{1}{c_a} \frac{p_{sat@T_l} - \varphi p_{sat@T_a}}{p - p_{sat@T_l}} \tag{4}$$

where the convection coefficient, h, can be evaluated from common relationships in the literature.

Due to the evaporative mass flux, the following boundary condition can be imposed on the heat flux across the liquid-air interface:

$$k_l \frac{\partial T_l}{\partial n} = h(T_l - T_a) + m'' \Lambda_l - q''_{rad} \tag{5}$$

The conditions on the top surface of the solid outside the droplet and on the bottom surface are:

$$k_s \frac{\partial T_s}{\partial z} = h(T_s - T_a) - q''_{rad} \tag{6}$$

In the present problem, the vertical surfaces of the solid are considered adiabatic; in particular, two surfaces are symmetry planes.

The boundary conditions at the solid-liquid interface state the continuity of temperature and heat flux:

$$T_l = T_s \tag{7}$$

$$k_l \frac{\partial T_l}{\partial z} = k_s \frac{\partial T_s}{\partial z} \tag{8}$$

The spherical-cap-shaped droplet is initially symmetrical about the vertical axis, perpendicular to the surface of the substrate.

The described 3D model has been coded in Matlab® to obtain a transient temperature profile on the substrate surface, that could be compared with the thermographic experimental measurements. A structured non-uniform mesh is used, which is refined where the strongest temperature gradients and largest heat fluxes are expected (that is, at the interfaces and below the droplet). The elements in the droplet have different height, to consider the spherical-cap geometry.

The governing equations for the liquid and the solid substrate are discretized by finite volumes, with Crank-Nicolson for the time-advancement. An explicit approach is used to evaluate the liquid loss due to evaporation, as well as the heat transfer coefficient and the material properties at each node and time.

In particular, at every time step, the evaporated mass flux at the liquid-air interface is calculated for every top cell area, and the droplet is built and meshed again, considering the new amount of non-evaporated liquid.

The discretized computational domain for this code is shown in Fig. 8, where the droplet and the top surface of the solid layer at the beginning of transient simulation are depicted. The difference between the initial droplet volume and the reconstructed volume is less than -0.0014421 %.

Some preliminary results for single droplet evaporative transients are reported in Figs. 9 to 14. In those figures, the calculated temperature of the lower layer of the paint and of the upper layer of the BaF_2 disk are plotted versus time (Figs. 9-14) or radial

distance (Figs. 12-14) during different evaporative transients, and the numerical predictions are compared with the corresponding data from experimental measurements.

Figure 9 reports a comparison between experimental data and numerical predictions for the temperature transient of a solid surface point very close to the center of the droplet. Both experimental data and numerical calculations stress out the sudden temperature decrease right after the droplet deposition; the code predictions tend to overestimate the solid surface temperature evolution immediately after the droplet deposition, but during the following portion of the transient the temperature evolution is well predicted.

Figures 10 and 11 report the same comparison of Fig. 9 for the temperature transient of a solid surface point located a 3.0 mm and 4 mm from the center of the droplet respectively. Again, both experimental data and numerical calculations stress out the sudden temperature decrease right after the droplet deposition; in these cases the numerical results show a good agreement during the whole portion of the transient considered.

Figures 12, 13 and 14 report the comparisons between experimental data and numerical predictions for the solid surface temperature distribution along the radial coordinate from the droplet center, x, at three different times, starting with the first instant after droplet deposition. The agreement appears to be satisfactory in the non-wetted area even if the code tends to slightly overestimate the solid surface temperature (Figs. 13-14).

In the challenging zone of the wetted area, the same discrepancies observed in the temperature vs. time plots of Figs. 9-11 affect the temperature vs.distance plots of Figs. 12-14. In particular, the code tends to overestimate the temperature in the central zone of the droplet in the first instants of the evaporation (Fig. 12); in the remaining part of

the transient (Figs. 13-14) a better agreement is evident even if at the edge of the droplet the measured temperatures are lower than the predicted ones. An improvement of predictive capabilities of both model and code is going to be attempted on the basis of more complete information from the experimental measurements.

CONCLUDING REMARKS

In order to analyze the cooling of hot solid surfaces induced by liquid droplets, an approach to non-intrusive measurement of the transient contact temperature between impinging droplets and hot solid surfaces has been presented. The solid-liquid interface temperature has been monitored from below through a transparent-to-infrared material. That material had been coated with a very thin layer of high-emissivity, opaque paint on its upper side, so that it could effectively respond to the infrared camera located below.

The experimental results concerning transient temperature distributions confirmed many typical trends of dropwise cooling, and the direct observation of the solid-liquid interface temperature enhanced the comprehension of the phenomenology of the interactions between droplets and hot surfaces.

A numerical code has been presented, which simulates the evaporation of water droplets on hot solid surfaces. At the present stage of development, only single-phase evaporation has been addressed. The three-dimensional energy diffusion equation, discretized using the finite volume method, has been employed to model the transient within both the droplets and the solid substrate. The numerical results have been compared with the experimental data. The preliminary results showed good agreement but also some relevant discrepancies between code predictions and experimental data. However, the present contribution can only be considered the starting point for the development of more complex and versatile models for the simulation of multi-droplet systems. Several phenomena, such as convective motion and nucleate boiling within the droplet, radiative heat transfer, high Weber numbers and different impingement modes, will be progressively included into the numerical simulation. The enhanced modeling

capabilities will have to be accompanied by high-resolution experimental data for the validation of the code.

NOMENCLATURE

c	specific heat (J kg^{-1} K^{-1})
d_{aw}	air-water mass diffusivity (m^2 s^{-1})
k	thermal conductivity (W m^{-1} K^{-1})
h	heat transfer coefficient (w m^{-2} K^{-1})
m”	vapor mass flux (kg s^{-1} m^{-2})
n	normal coordinate (m)
p	pressure (Pa)
q"	heat flux (W m^{-2})
R	droplet (wetted area) radius (m)
T	temperature (°C or K)
t	time (s)
x	radial coordinate from the droplet center (m or mm)
z	vertical coordinate (m)

Greek letters

α	thermal diffusivity (m^2 s^{-1})
Δλ	spectral range (m or μm)
θ	solid-liquid contact angle (rad)
Λ	latent heat of vaporization (J kg^{-1})
λ	wavelength (m or μm)
ρ	mass density (kg m-3)
τ_λ	spectral transmittance
φ	relative humidity (-)

Subscripts

0	initial
a	air, ambient

contact	contact, interface
l	liquid
rad	radiative
s	solid
sat	saturation

ACKNOWLEDGMENTS

These studies were made possible by the financial contribution of the Italian M.I.U.R. All the students who worked on the experimental apparatus during the entire period of the present research are also acknowledged.

REFERENCES

[1] di Marzo, M. and Evans, D., Evaporation of a Water Droplet Deposited on a High Thermal Conductivity Surface, *ASME J. Heat Transfer*, 111 (1989), 210-213.

[2] di Marzo, M., Tartarini, P., Liao, Y., Evans D. and Baum, H., Dropwise Evaporative Cooling, *ASME HTD*, 166 (1991), 51-58.

[3] di Marzo, M., Tartarini, P., Liao, Y., Evans, D. and Baum, H., Evaporative Cooling Due to a Gently Deposited Droplet, *Int. J. Heat Mass Transfer*, 36 (17) (1993), 4133-4139.

[4] Tartarini, P. and di Marzo, M., Mixed Numerical Scheme Solution for Dropwise Evaporative Cooling, *Advanced Computational Methods in Heat Transfer III*, Editors: L.C. Wrobel, C.A. Brebbia, A.J. Nowak, Computer Mechanics Publications, pp. 473-480, 1994.

[5] Chandra, S., di Marzo, M., Qiao, Y.M. and Tartarini, P., Effect of Liquid-Solid Contact Angle on Droplet Evaporation, *Fire Safety Journal*, 27 (1996), 141-158.

[6] Tartarini, P., Lorenzini, G., Randi, M.R. and di Marzo, M., Experimental and Numerical Study on Evaporative Spray Cooling of Hot Surfaces, *Proc. of the 4th World Conference on Experimental Heat Transfer, Fluid Mechanics and Thermodynamics*, Brussels, Belgium, pp. 1319-1326, 1997.

[7] Tarozzi, L., Muscio, A. and Tartarini, P., Dropwise Cooling: Experimental Tests on Infrared-Transparent Media, *Proc. 23rd UIT National Heat Transfer Conference*, Parma, Italy, pp. 269-274, 2005.

[8] Tarozzi, L., Muscio, A. and Tartarini, P., Experimental tests of dropwise cooling on infrared-transparent media, *Exp. Thermal and Fluid Science*, 31 (2007), 857-865.

[9] Gorton, C.W., Heat Transfer to Drops of Liquid in the Spheroidal State, PhD Thesis, Purdue University, West Lafayette, IN, USA, 1953.

[10] Wachters, L.H.J., Bonne, H. and Van Nouhuis, H.J., The Heat Transfer from a Hot Horizontal Plate to Sessile Drops in the Spheroidal State, *Chem. Eng. Science*, 21 (1966), 923-936.

[11] Baumeister, K.J., Hamill, T.D., Schwartz, F.L. and Schoessow, G.J., Film Boiling Heat Transfer to Water Drops on a Flat Plate, *Chem. Eng. Prog. Symp. Ser.*, 62 (1973), 52-61.

[12] Bolle, L. and Moureau, J.C., Spray Cooling of Hot Surfaces, in G.F. Hewitt, J.M. Delhaye and N. Zuber (ed.) Multiphase Science and Technology, pp. 1-92, Hemisphere, New York, 1976.

[13] Chandra, S. and Avedisian, C.T., On the Collision of a Droplet with a Solid Surface, *Proc. Royal Soc. London*, 432 (1991), 13-41.

[14] Wachters, L.H.J. and Westerling, N.A.J., The Heat Transfer from a Hot Wall to Impinging Water Drops in the Spheroidal State, *Chem. Eng. Science*, 21 (1966), 1047-1056.

[15] Adam, N. and Jessop, G., Angles of Contact and Polarity of Solid Surfaces, *J. Chem. Soc*., 127 (1925), 1863-1868.

[16] Good, R.J., A Thermodynamic Derivation of Wenzel's Modification of Young's Equation for Contact Angles; Together with a Theory of Hysteresis, *J. Colloid Interface Science*, 74 (1952), 5041-5042.

[17] Herzberg W.J. and Marian, J.E., Relationship Between Contact Angle and Drop

Size, *J. Colloid Interface Science*, 33 (1970, 161-163.

[18] Herzberg W.J., Marian, J.E. and Vermeulen, T., The Receding Contact Angle, *J. Colloid Interface Science*, 33 (1970), 164-171.

[19] Bernardin, J.D., and Mudawar, I., Film Boiling Heat Transfer of Droplet Streams and Sprays, *Int. J. Heat Mass Transfer*, 40 (11) (1997), 2579-2593.

[20] Bernardin, J.D., Stebbins, C.J. and Mudawar, I., Mapping of Impact and Heat Transfer Regimes of Water Drops Impinging on a Polished Surface, *Int. J. Heat Mass Transfer*, 40 (2) (1997), 247-267.

[21] Sikalo, S., Marengo, M., Tropea C. and Ganic, E.N., Analysis of impact of droplets on horizontal surfaces, *Exp. Thermal and Fluid Science*, 25 (2002), 503-510.

[22] Cossali, G.E., Marengo, M. and Santini, M., Secondary atomisation produced by single droplet vertical impact onto heated surfaces, *Exp. Thermal and Fluid Science*, 29 (2005), 937-946.

[23] Crystran Ltd, Barium Fluoride (BaF_2) – Product Data, available on the web: www.crystran.co.uk/products.asp?productid=75.

[24] Seki, M., Kawamura, H. and Sanokawa, K., Transient Temperature Profile of a Hot Wall Due to an Impinging Liquid Droplet, *ASME J. Heat Transfer*, 100 (1978), 167-169.

[25] Carslaw, H.S. and Jaeger, J.C., Conduction of Heat in Solids, Clarendon Press, Oxford, UK, 1959.

[26] Abu-Zaid, M. and Atreya, A., Transient Cooling of Hot Porous and Nonporous Ceramic Solids by Droplet Evaporation, *ASME J. Heat Transfer*, 116 (1994), 694-701.

[27] Rizza, J.J., A Numerical Solution to Dropwise Evaporation, *ASME J. Heat*

Transfer, 103 (1981), 501-507.

[28] Wrobel, L.C. and Brebbia, C.A., A Formulation of the Boundary Element Method for Axisymmetric Transient Heat Conduction, *Int. J. Heat Mass Transfer*, 24 (5) (1981), 843-850.

[29] Chilton, T.H. and Colburn, A.P., Mass transfer (adsorption) coefficients prediction data on heat transfer fluid motion, *lnd. Eng. Chem.*, 26 (1934), 1183-1187.

FIGURE CAPTIONS

Figure 1 - Experimental apparatus.

Figure 2 - Experimental layout.

Figure 3 - Scheme of the test section.

Figure 4 - Spectral transmittance of the BaF_2 disk.

Figure 5 - Sequence of thermographic images: four droplets (45 μl each) on the BaF_2 disk; T_0= 97°C.

Figure 6 - Sequence of thermographic images: multi-droplet spray (180 μl) on the BaF_2 disk; T_0= 97°C.

Figure 7 - Comparison between experimental and predicted values of temperature vs. time on the wetted area.

Figure 8 - Discretized computational domain.

Figure 9 - Initial evolution of the top surface under the droplet at x = 0.21 mm from the center of the droplet (initial radius of the droplet = 4.5 mm).

Figure 10 - Initial evolution of the top surface under the droplet at x = 3.0 mm from the center of the droplet (initial radius of the droplet = 4.5 mm).

Figure 11 - Initial evolution of the top surface under the droplet at x = 4 mm from the center of the droplet (initial radius of the droplet = 4.5 mm).

Figure 12 - Temperature distribution along the x-axis right after droplet deposition.

Figure 13 - Temperature distribution along the x-axis at t=10s after droplet deposition.

Figure 14 - Temperature distribution along the x-axis at t=40s after droplet deposition.

FIGURES

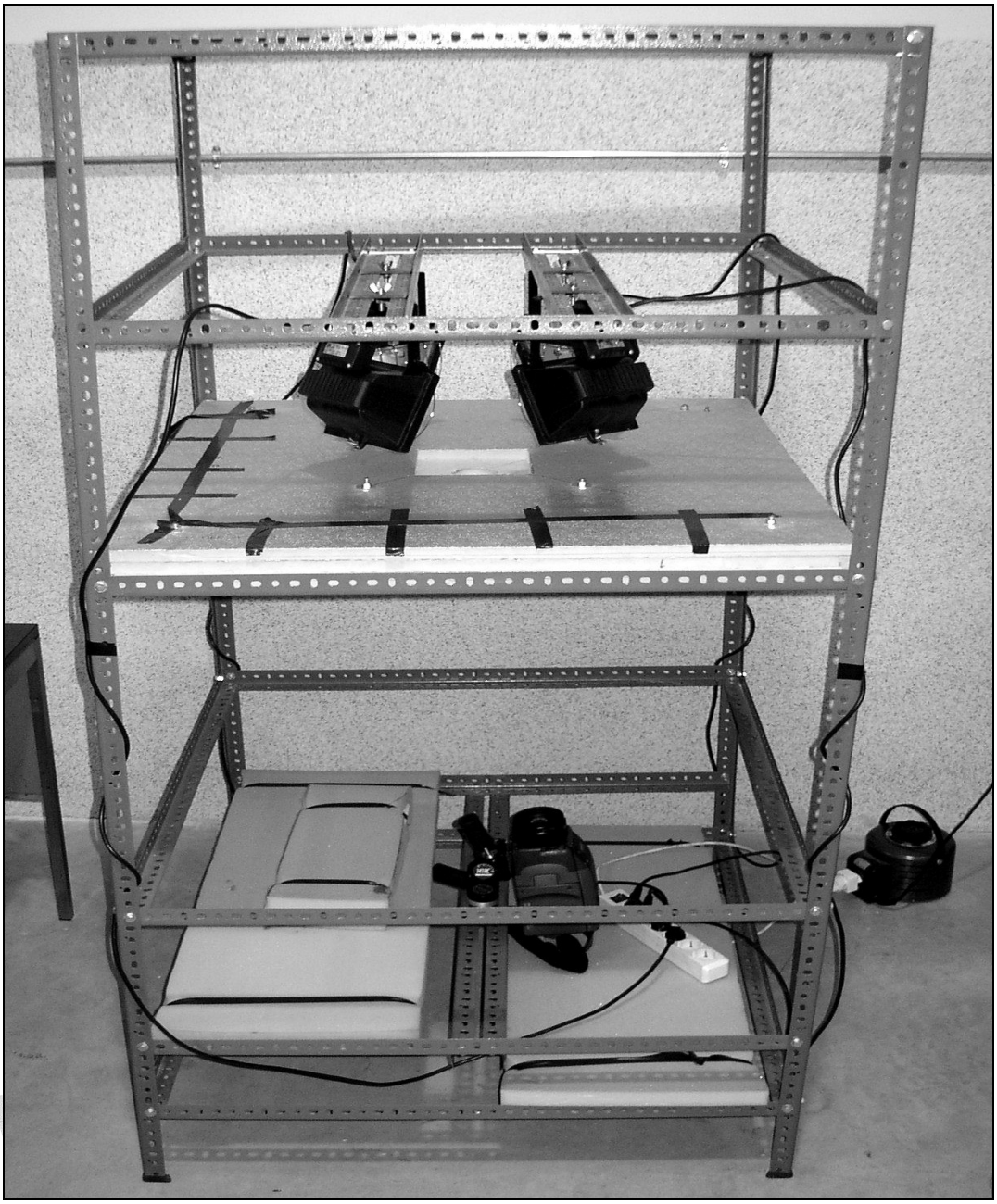

Figure 1 - Experimental apparatus.

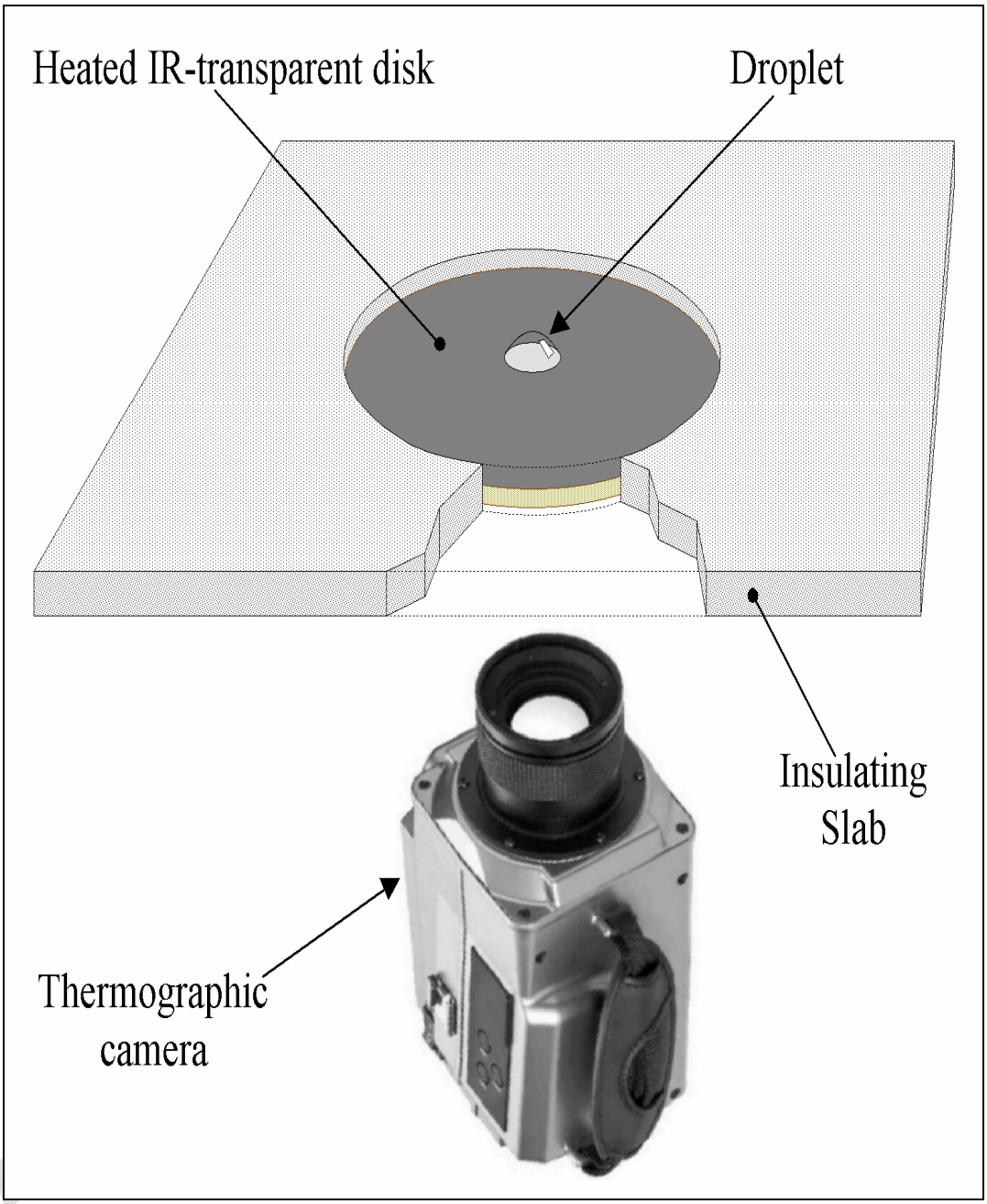

Figure 2 - Experimental layout.

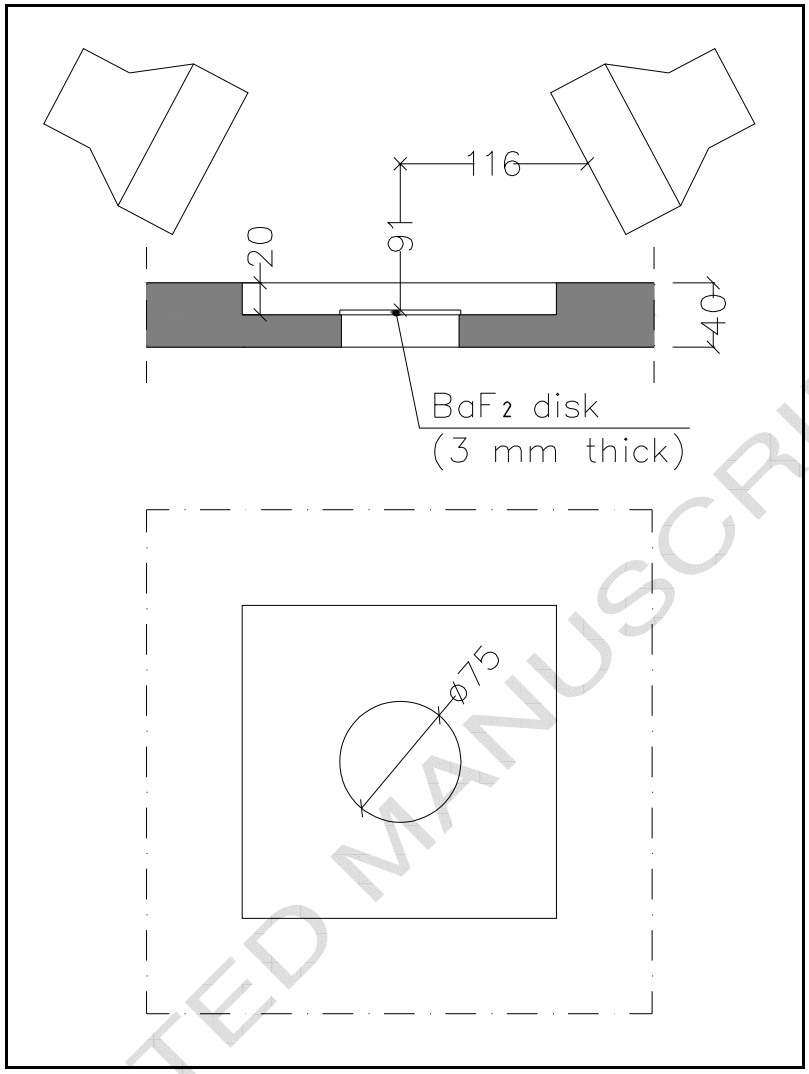

Figure 3 – Sketch of the test section.

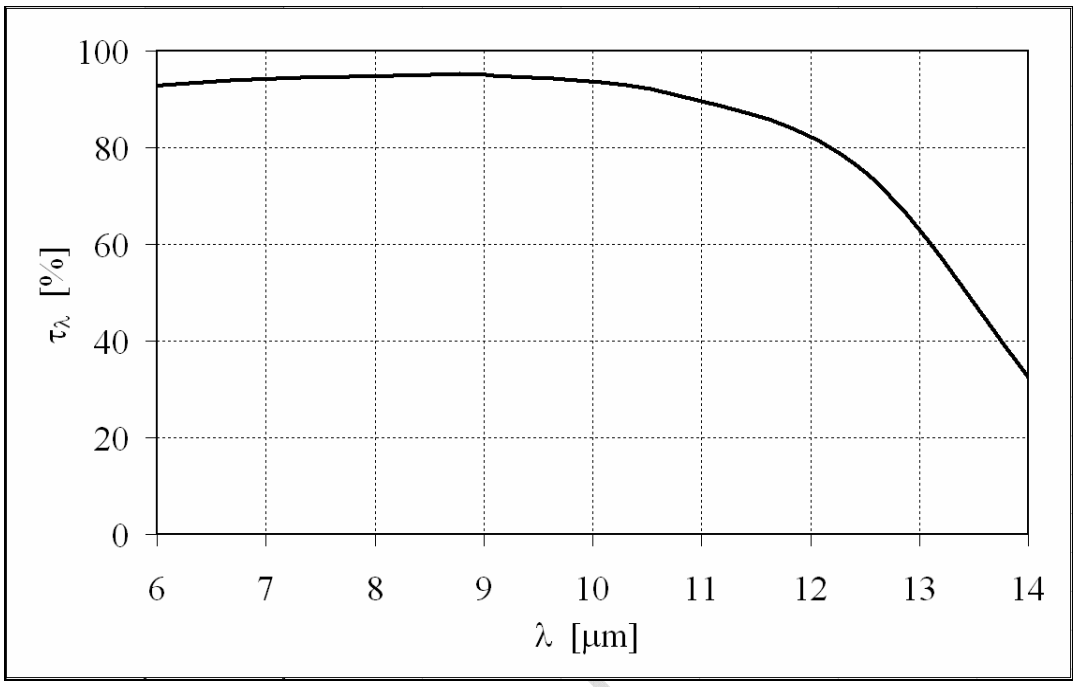

Figure 4 - Spectral transmittance of the BaF_2 disk.

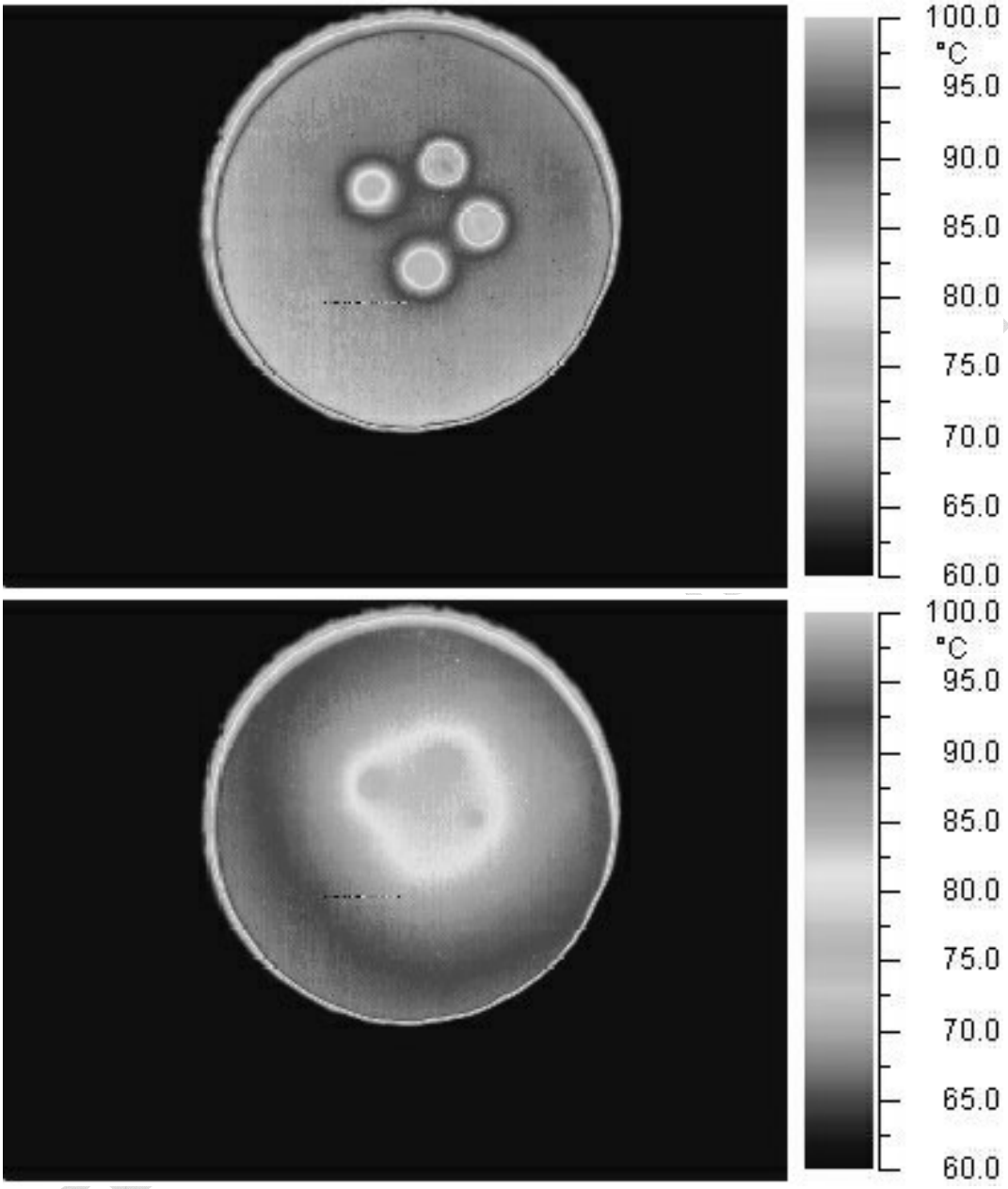

Figure 5 - Sequence of thermographic images: four droplets (45 µl each) on the BaF_2 disk; T_0= 97°C.

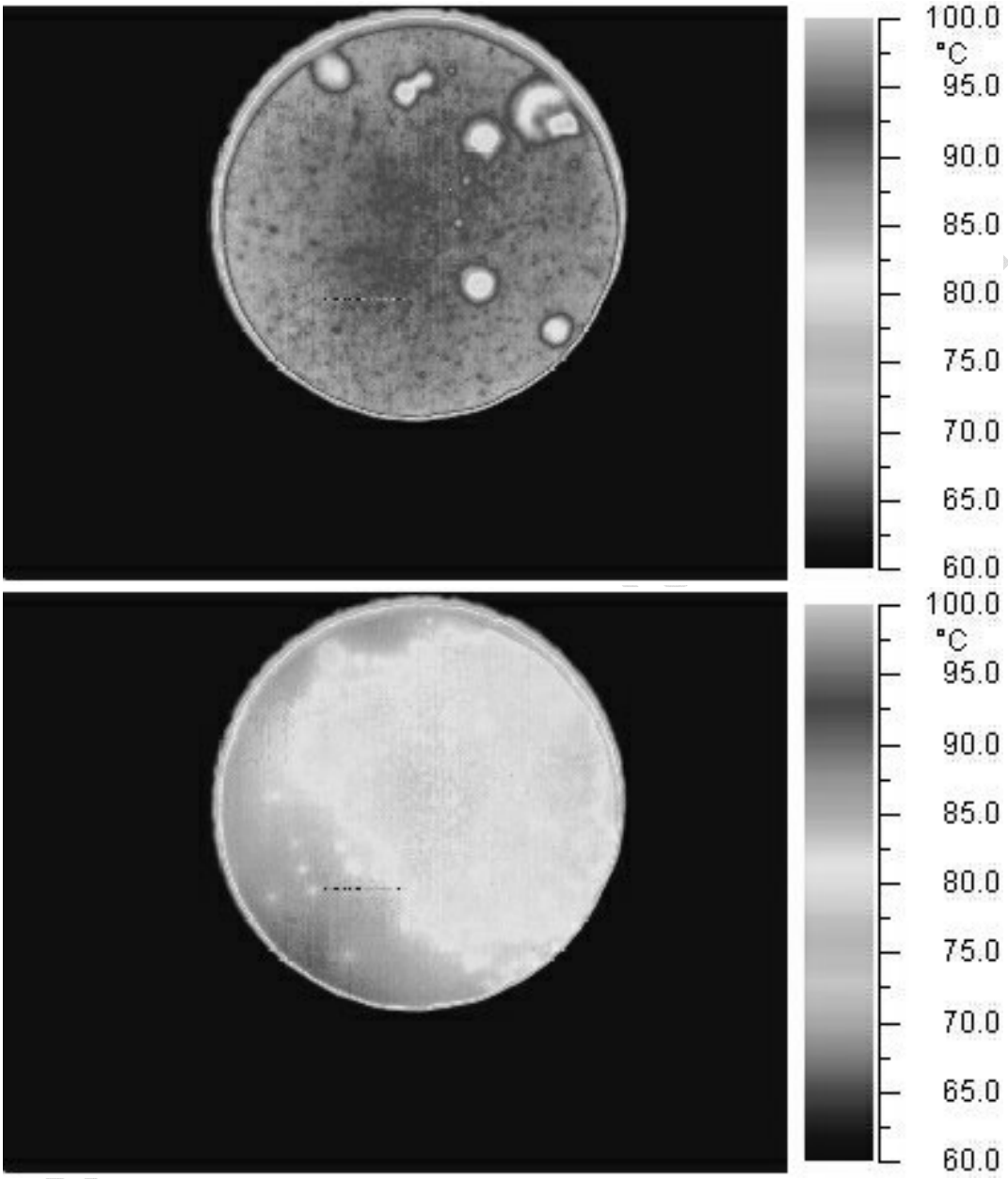

Figure 6 – Sequence of thermographic images: multi-droplet spray (180 µl) on the BaF_2 disk; T_0= 97°C.

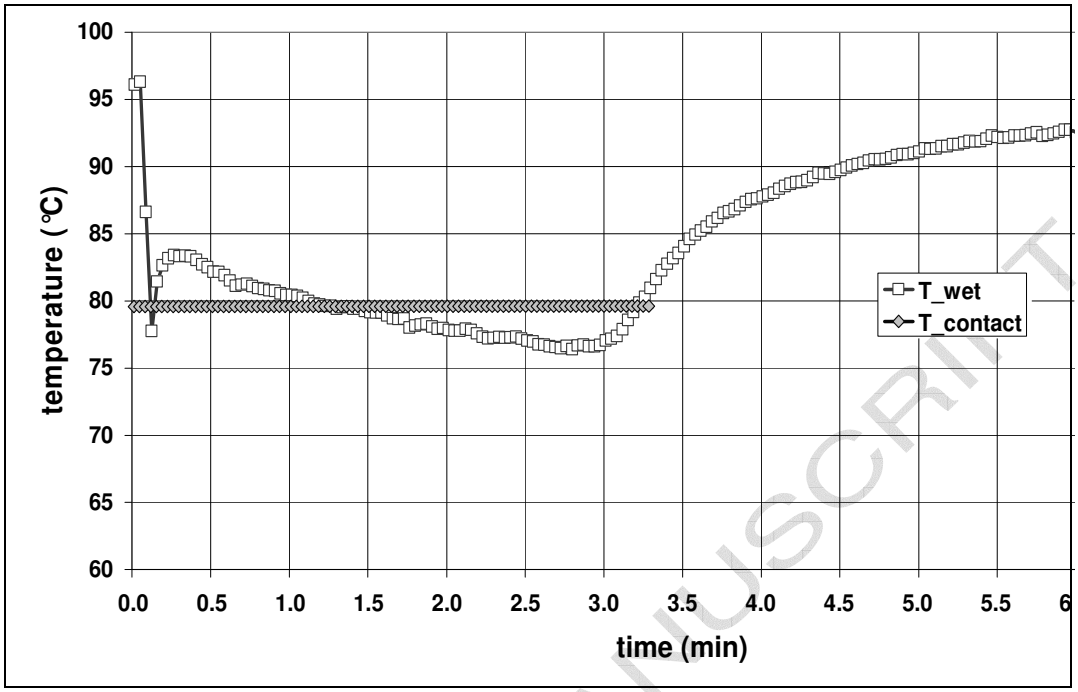

Figure 7 - Comparison between experimental and predicted values of temperature vs. time on the wetted area.

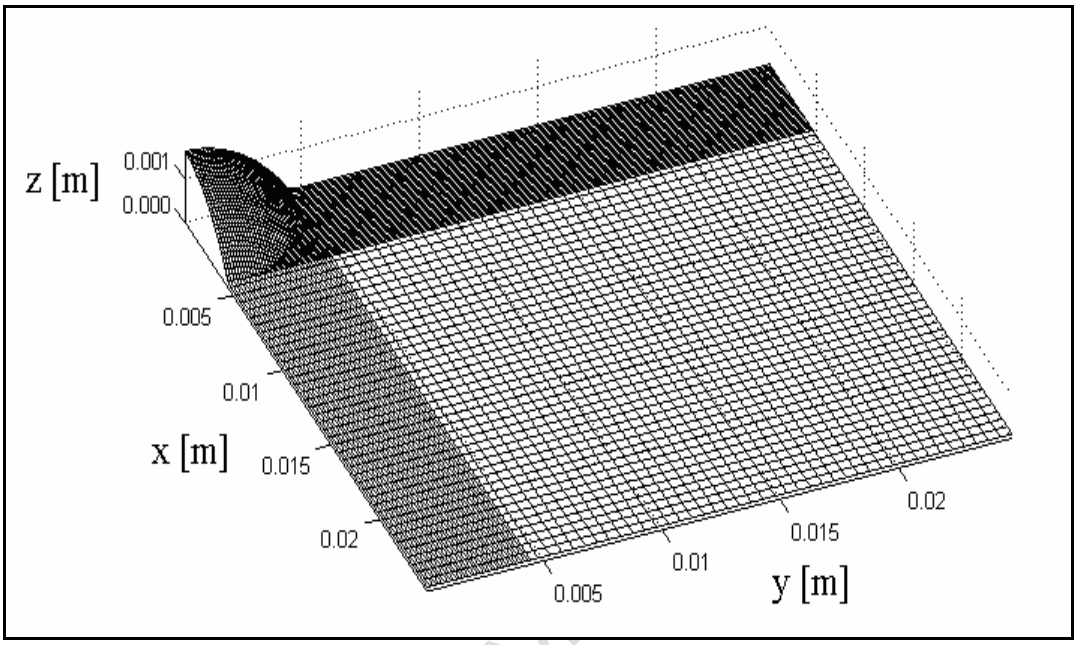

Figure 8 – Discretized computational domain.

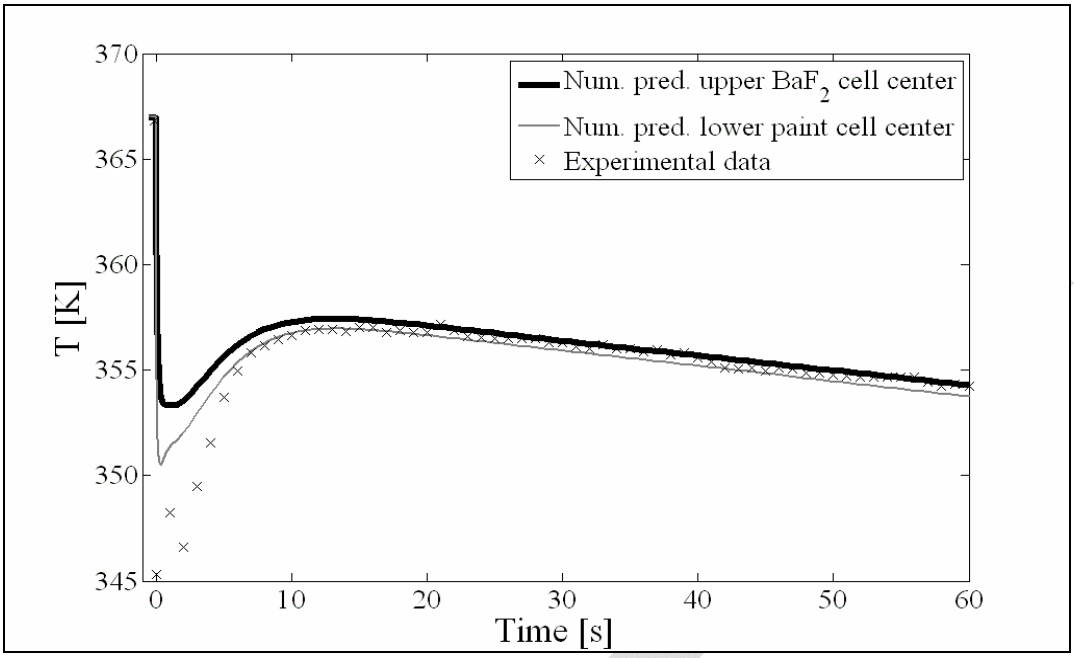

Figure 9 - Initial evolution of the top surface under the droplet at x = 0.21 mm from the center of the droplet (initial radius of the droplet = 4.5 mm).

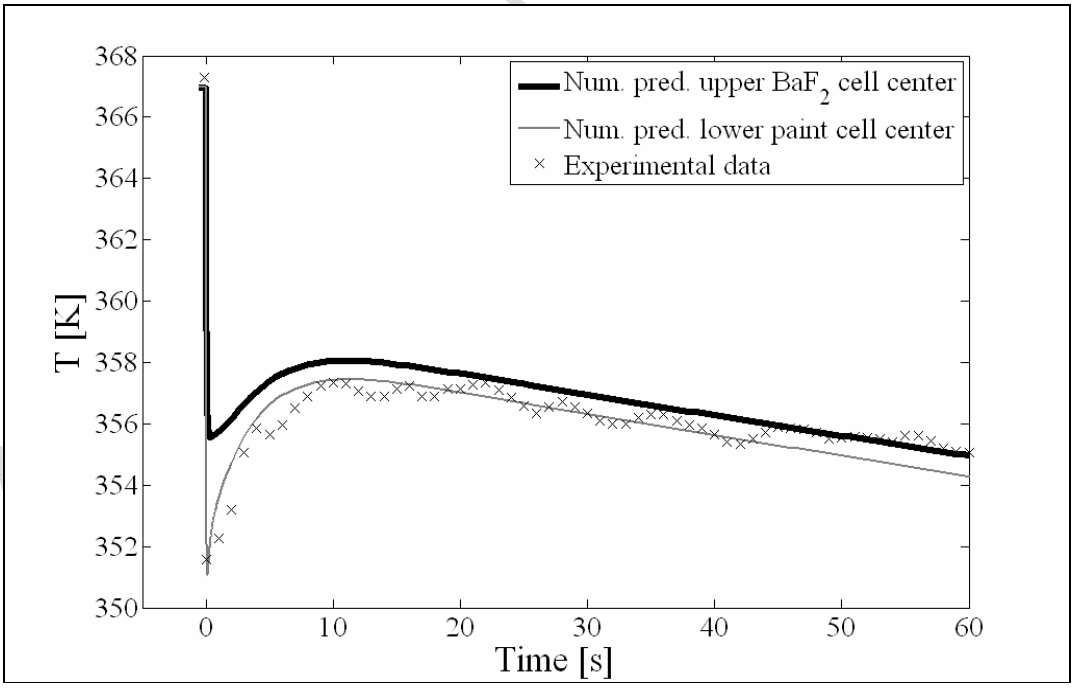

Figure 10 - Initial evolution of the top surface under the droplet at x = 3.0 mm from the center of the droplet (initial radius of the droplet = 4.5 mm).

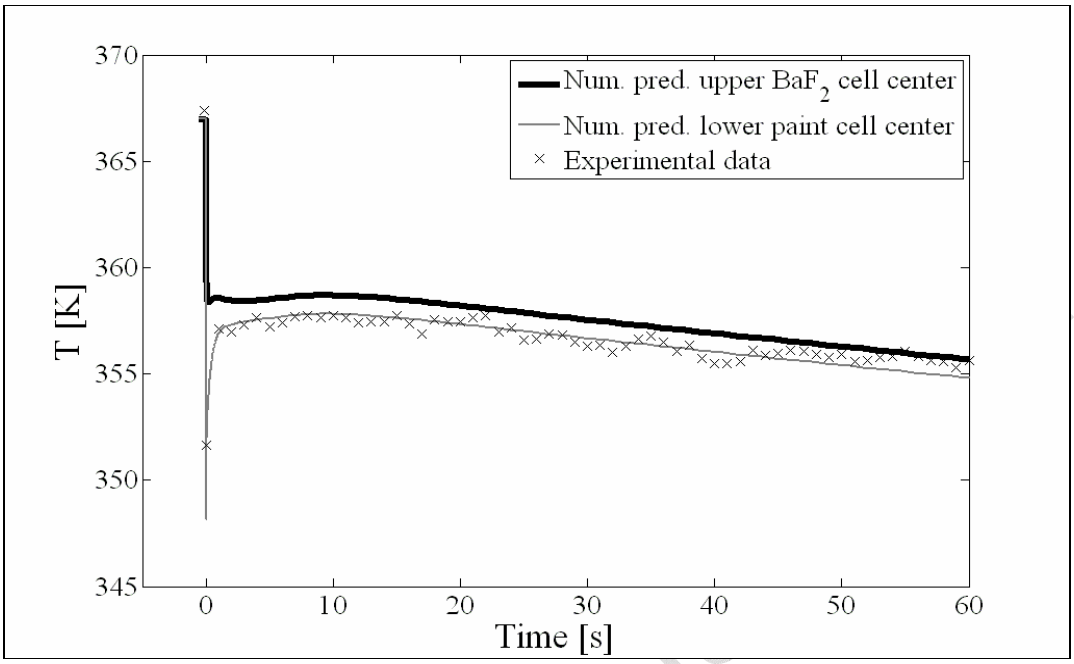

Figure 11 - Initial evolution of the top surface under the droplet at x = 4 mm from the center of the droplet (initial radius of the droplet = 4.5 mm).

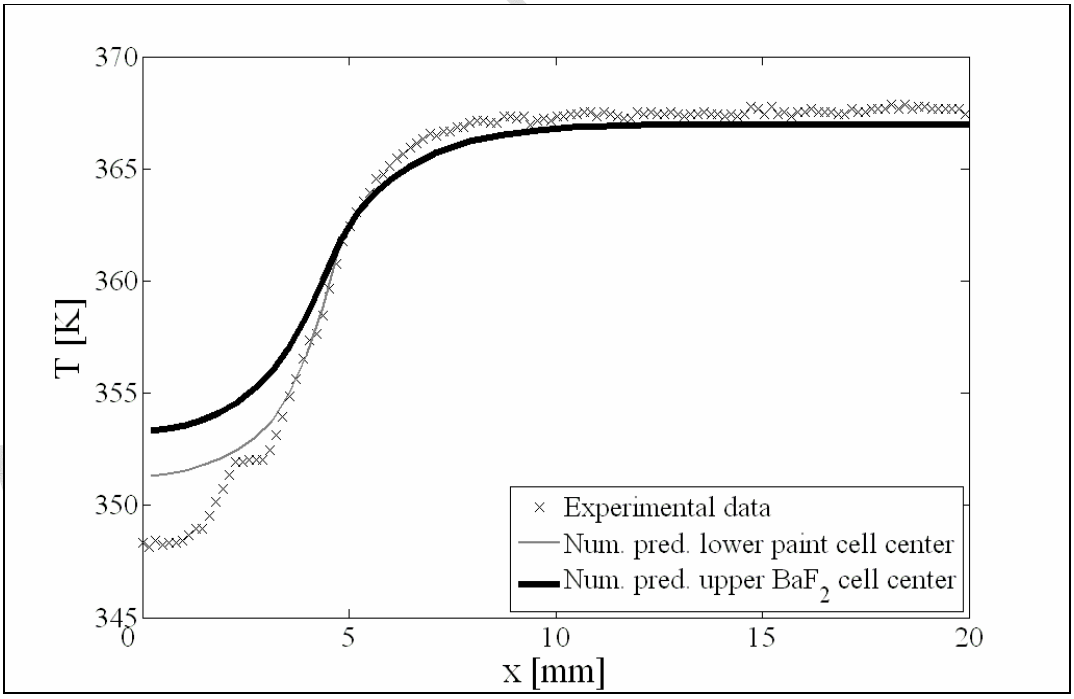

Figure 12 - Temperature distribution along the x-axis right after droplet deposition.

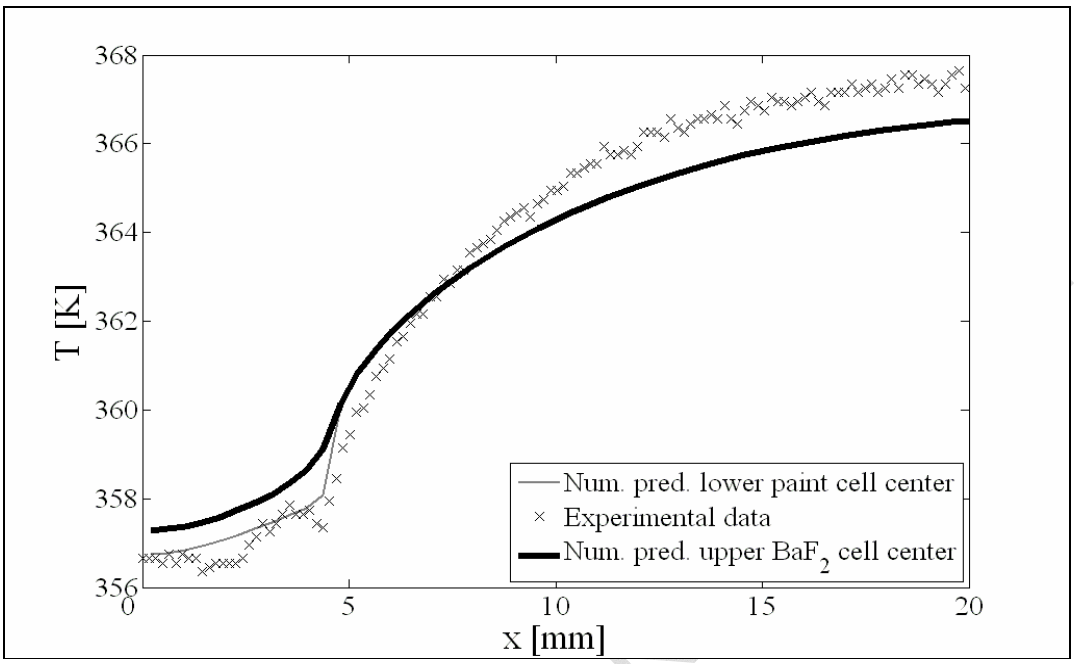

Figure 13 - Temperature distribution along the x-axis at t=10s after droplet deposition.

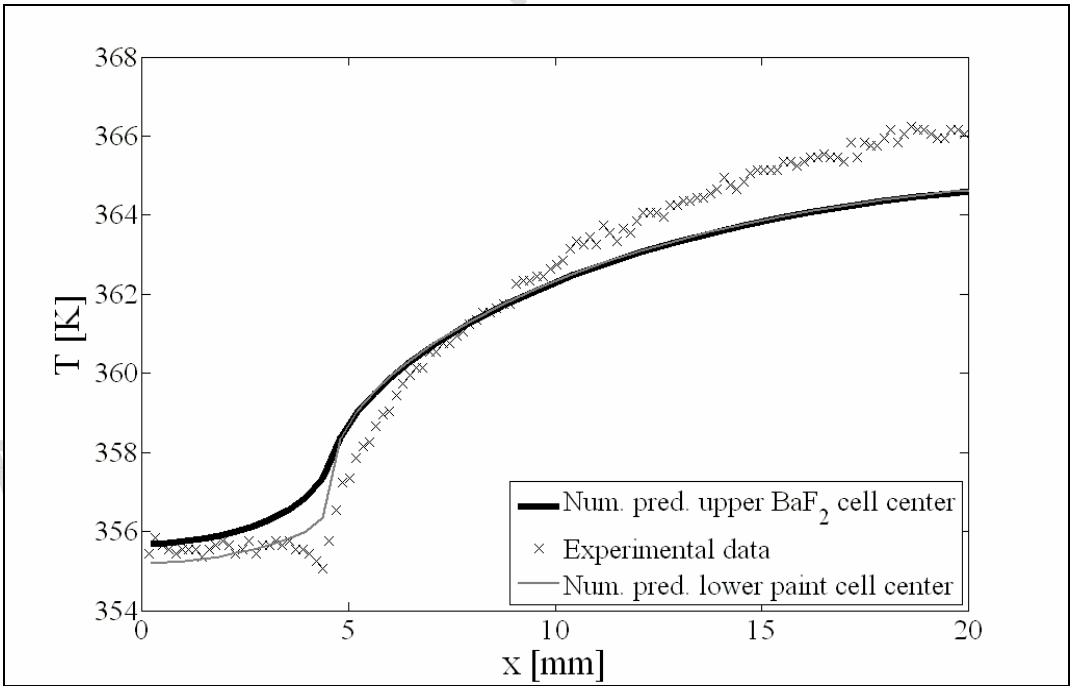

Figure 14 - Temperature distribution along the x-axis at t=40s after droplet deposition.